Supplementary Material

S1. Crystallization modeling

Equations 1 to 19 show the method of classes discretization for the solution of the same system, in a two-dimensional PBE:

for $i=1,\ldots,n$ and $j=1,\ldots,m$:

$$\frac{dN_{i,j}}{dt} + f_{i,j}(t) + f'_{i,j}(t) - f^{d}_{i,j}(t) - f^{d'}_{i,j}(t) = B - D \tag{1}$$

$$f_{i,j}(t) = f^{1,0}_{i,j}(t) - f^{1,I}_{i,j}(t) \tag{2}$$

$$f^{d}_{i,j}(t) = f^{d,1,0}_{i,j}(t) - f^{d,1,I}_{i,j}(t) \tag{3}$$

$$f'_{i,j}(t) = f^{2,0}_{i,j}(t) - f^{2,I}_{i,j}(t) \tag{4}$$

$$f^{d'}_{i,j}(t) = f^{d,2,0}_{i,j}(t) - f^{d,2,I}_{i,j}(t) \tag{5}$$

$$f^{1,0}_{i,j}(t) = G_x(a_i N_{i,j}(t) + b_i N_{i+1,j}(t)) \tag{6}$$

$$f^{d,1,0}_{i,j}(t) = D_x(a_i N_{i,j}(t) + b_i N_{i+1,j}(t)) \tag{7}$$

$$f^{1,I}_{i,j}(t) = G_x(a_{i-1} N_{i-1,j}(t) + b_{i-1} N_{i,j}(t)) \tag{8}$$

$$f^{d,1,I}_{i,j}(t) = D_x(a_{i-1} N_{i-1,j}(t) + b_{i-1} N_{i,j}(t)) \tag{9}$$

$$a_i = \frac{\triangle Cl_{i+1}}{\triangle Cl_i(\triangle Cl_{i+1} + \triangle Cl_i)} \tag{10}$$

$$b_i = \frac{\triangle Cl_i}{\triangle Cl_i(\triangle Cl_{i+1} + \triangle Cl_i)} \tag{11}$$

$$f_{i,j}^{2,0}(t) = G_y(c_i N_{i,j}(t) + d_i N_{i+1,j}(t)) \tag{12}$$

$$f_{i,j}^{d,2,0}(t) = G_y(c_i N_{i,j}(t) + d_i N_{i+1,j}(t)) \tag{13}$$

$$f_{i,j}^{2,0}(t) = G_y(c_{i-1} N_{i-1,j}(t) + d_{i-1} N_{i,j}(t)) \tag{14}$$

$$f_{i,j}^{d,2,0}(t) = D_y(c_{i-1} N_{i-1,j}(t) + d_{i-1} N_{i,j}(t)) \tag{15}$$

$$f_{i,j}^{2,I}(t) = G_y(c_{i-1} N_{i-1,j}(t) + d_{i-1} N_{i,j}(t)) \tag{16}$$

$$f_{i,j}^{d,2,I}(t) = D_y(c_{i-1} N_{i-1,j}(t) + d_{i-1} N_{i,j}(t)) \tag{17}$$

$$c_i = \frac{\triangle Cl_{j+1}}{\triangle Cl_j(\triangle Cl_{j+1} + \triangle Cl_j)} \tag{18}$$

$$d_i = \frac{\triangle Cl_j}{\triangle Cl_{j+1}(\triangle Cl_{j+1} + \triangle Cl_j)} \tag{19}$$

S2. Golden Batch Simulation Results

Figure S1 shows the concentration profile and the 2-dimensional CSD for the Ibuprofen crystallization, after a 5 hours crystallization.

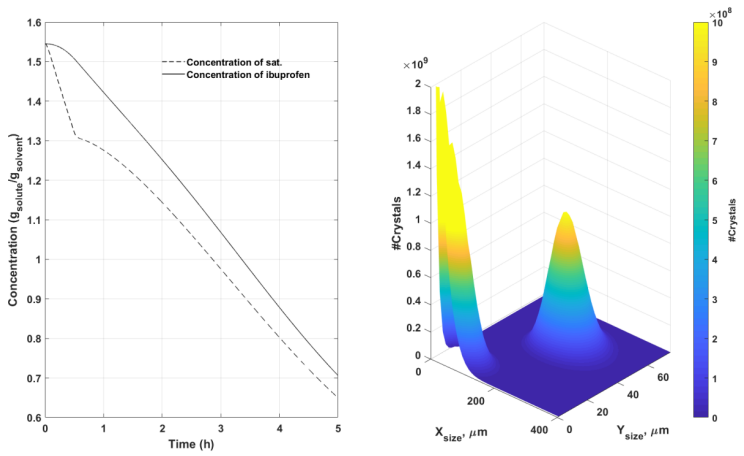

Figure S1. Ibuprofen solute concentration and saturation profile over the 5 hours crystallization(left), and CSD of ibuprofen crystal after 5 hours crystallization (right).

The target production of Ibuprofen was of roughly 50 kg per batch, with the available solubility dynamics. However, as shown in Figure S1 , the slow growth dynamics do not allow the solute concentration to reach the solubility curve, and the final process saturation is $0.69 kg/kg_{solvent}$, instead of the expected 0.65 $kg/kg_{solvent}$ for the 12°C end temperature. In addition, as can be observed, the CSD shows a huge population peak within the lower size part of the classes grid. This phenomenon occurs due to secondary nucleation, and creates a population of smaller particles with off-spec attributes. With the target of having crystals bigger than 150μm characteristic length and 70μm characteristic width, the final crystallization results are shown in Table S1.

Table S1. Ibuprofen crystallization final results.

Crystallizer volume (L)	60
Initial mass of Ibuprofen (kg)	82.08
Seed added (kg)	2.52
Final mass obtained (kg)	48.1
Final mass expected 8kg)	50.6
Non-crystallized ibuprofen mass	31.5
Underspecified Ibuprofen (kg)	3.14

The real mass of Ibuprofen obtained is approximately 45.6 kg per batch, as the initial seed

needs to be deducted. Removing the Ibuprofen that does not meet specifications, the total amount of produced Ibuprofen is 42.4 kg per batch, approximately 7.07 kg/hr. The yield of specified Ibuprofen is 51.7%, which for the process design proposed (20 degree cooling over 5 hours) is a considerable positive feature.

S3. RBF strategies for crystallization process

S3.1. Moving Window methodology

Figure S2 shows the workflow of the Moving Window methodology:

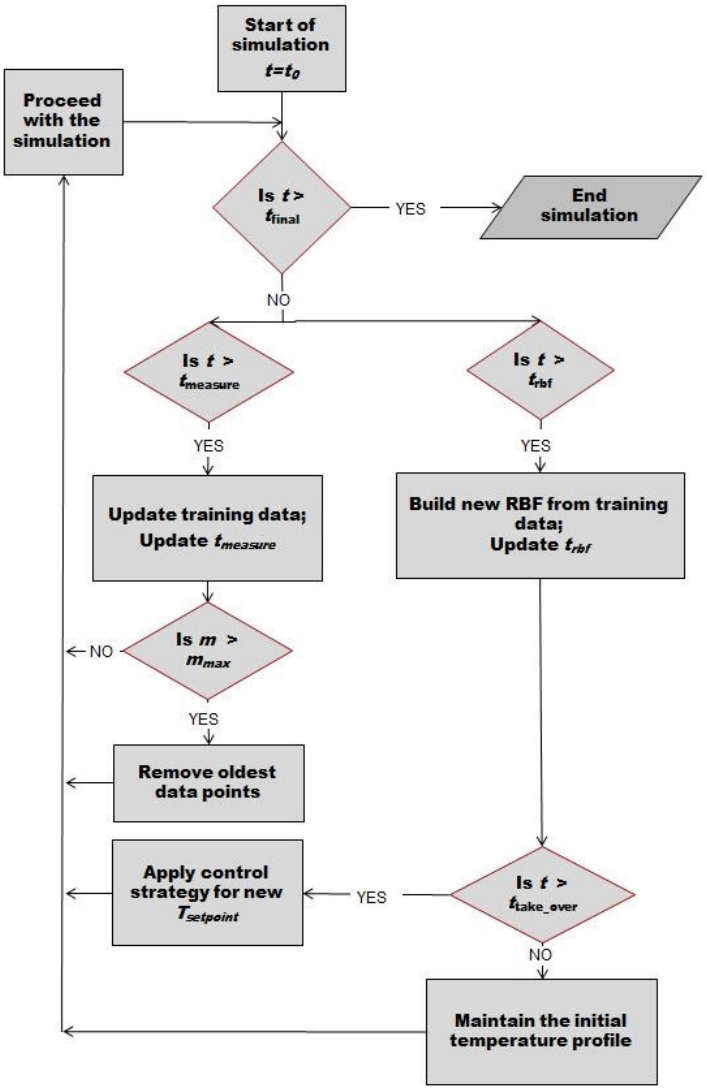

Figure S2. Workflow used to apply the RBF Moving Window methodology to crystallization.

S3.2. Golden Batch methodology

Figure S3 shows the workflow of the Golden Batch methodology:

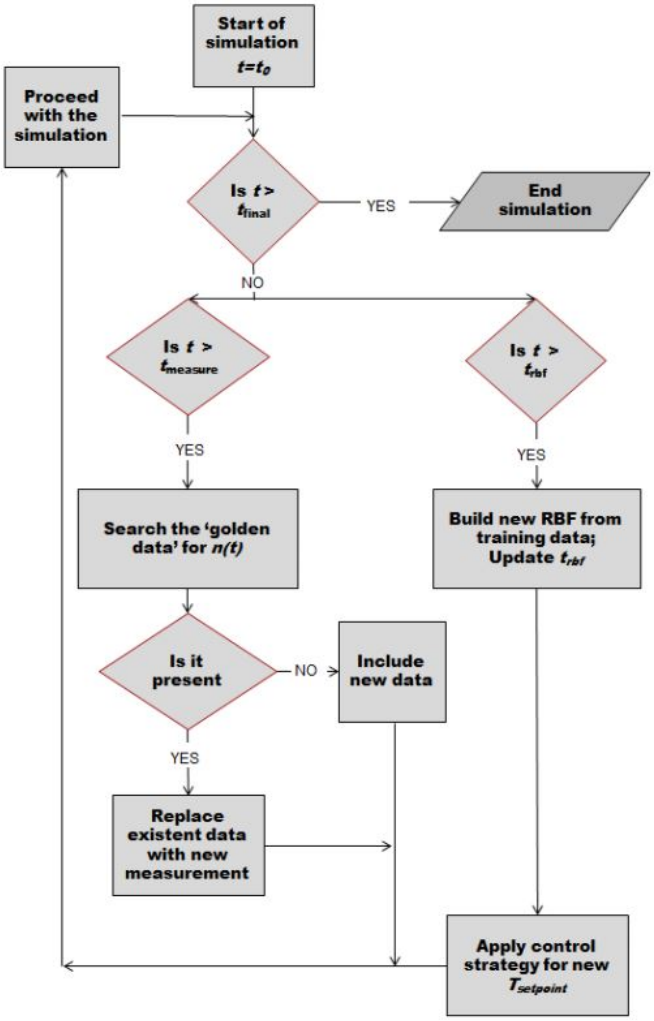

Figure S3. Workflow used to apply the RBF Golden Batch methodology to crystallization.

S4. RBF validation

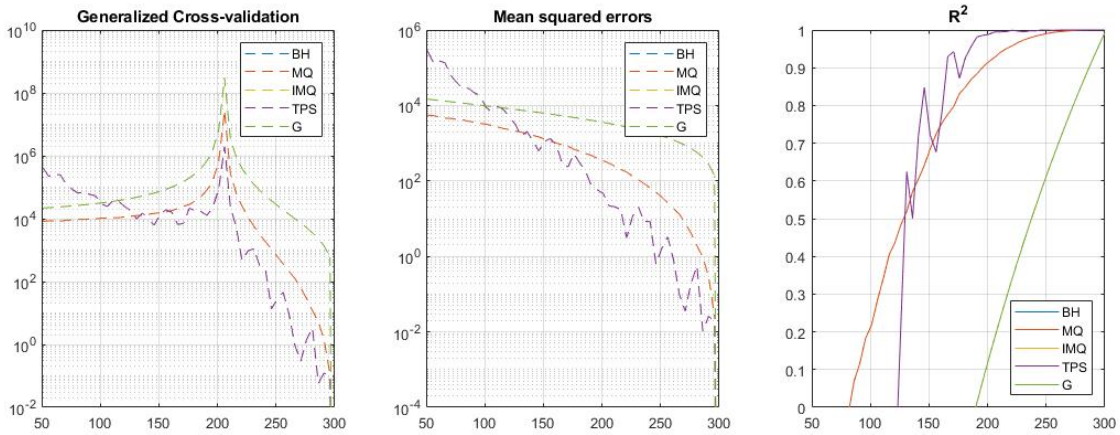

Figure S4. Decrease of the MSE and *gcv* (logarithmic scale) and increase of the R^2 with the expansion of the training data.

Figure S5 shows the output space for the different RBF transfers functions while seeding noise within its training data, and also the residual/deviation plotting from the target mean size for each respective RBF.

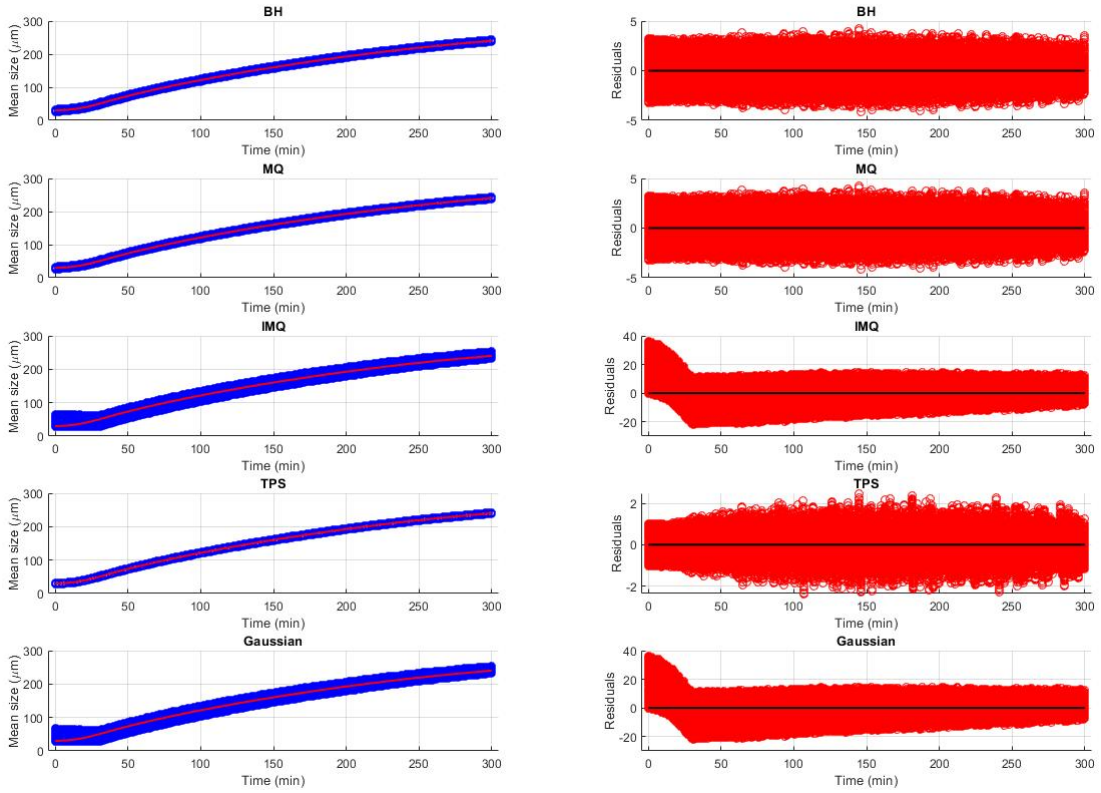

Figure S5. Predicted space of different RBF transfer functions with noise inputs and corresponding residuals.

Table S1. Scores for the performance of RBF transfer functions under training data noise

	Average R^2	**Lowest R^2**	**Average *MSE***	**Highest *MSE***
BH	0.9993	0.9992	2.362	2.532
MQ	0.9994	0.9992	2.360	2.531
IMQ	0.9809	0.9764	79.405	96.727
TPS	0.9999	0.9998	0.498	0.565
Gaussian	0.9807	0.9763	79.510	96.835

S5. Results obtained from RBF methodologies implemented within a PI soft sensor application

S5.1. Moving Window PI soft sensor application

Table S2. Evaluation metrics for the undisturbed crystallization controlled under RBF PI Moving window and traditional PI control methodologies.

Evaluation metric	**Units**	**Traditional PI**	**Moving Window RBF PI**
Final mean size	μ_m	238.2	238.6
IAE	$10^3\mu_m$	1.45	1.80
W_{IAE}	$10^7\mu_m$ min	3.47	2.85

S5.2. Growing Window PI soft sensor application

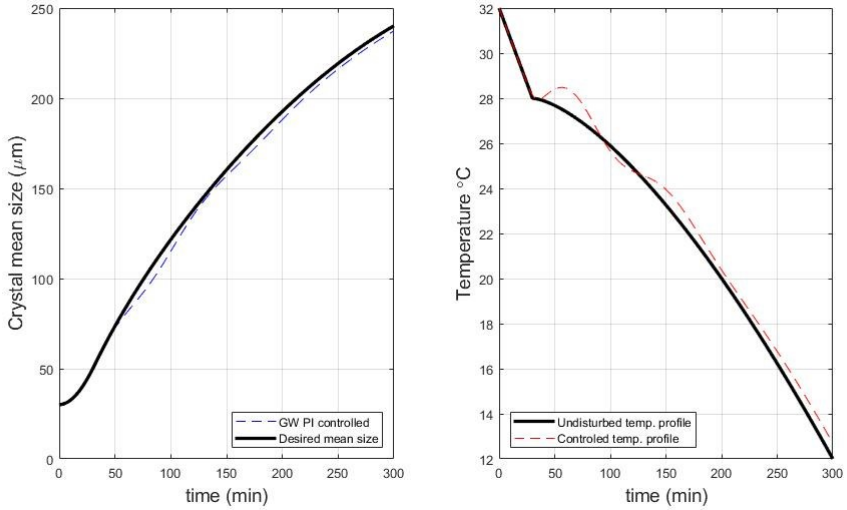

Figure S6. Crystal mean size (left) and temperature profile (right) obtained for the application of the Growing Window methodology to the RBF soft sensor for the undisturbed case scenario.

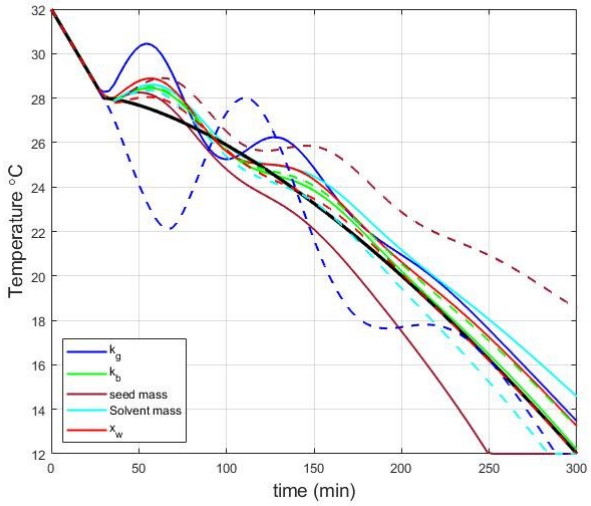

Figure S7. Controlled temperature profiles obtained for the application of the Growing Window methodology to the RBF soft sensor with single step disturbances (positive disturbance: full line; negative disturbance: dashed line

.

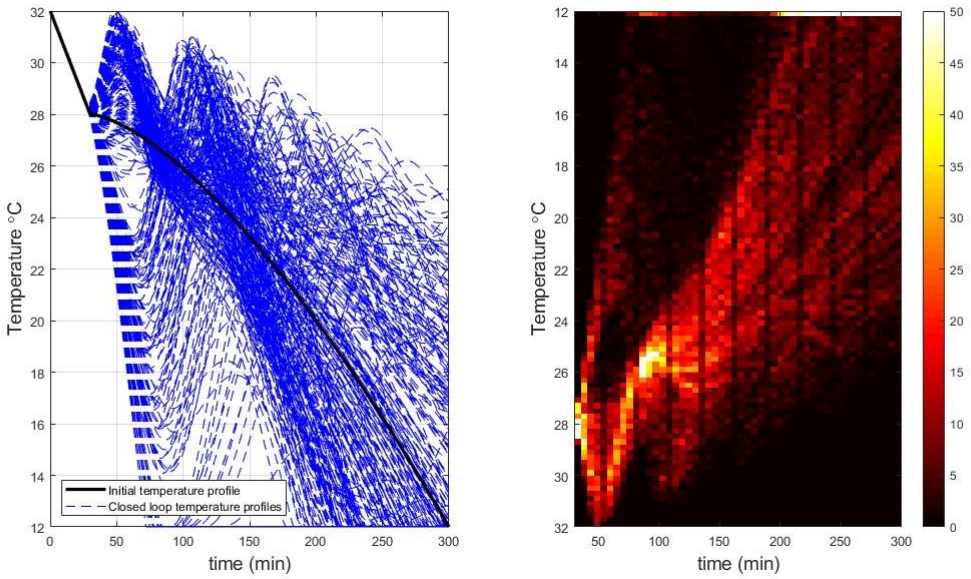

Figure S8. Controlled temperature profiles (left) and heat map of the temperature profiles over the course of the simulations (right) obtained for the application of the Growing Window methodology to the RBF soft sensor with Monte Carlo sampling disturbances (300 LHS samples simulated).

S5.3. Golden Batch PI soft sensor application

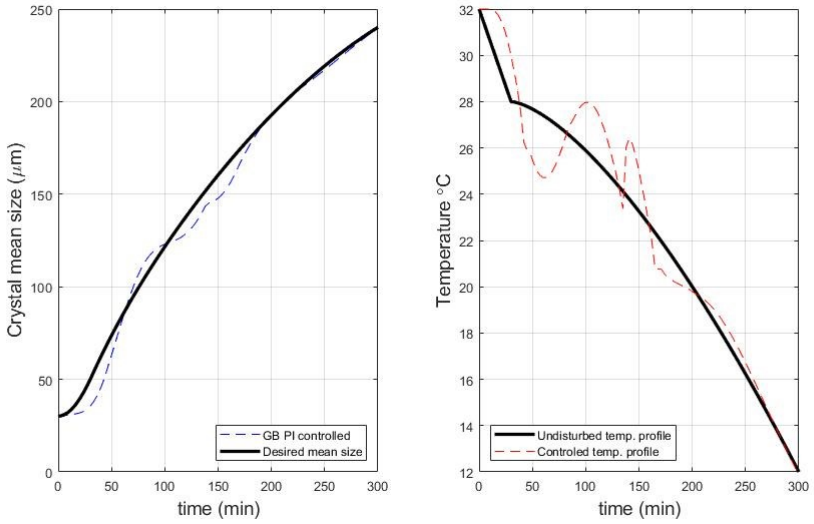

Figure S9. Controlled crystal mean size (up left), open loop crystal mean size (left) and temperature profile (right) obtained for the application of the Golden Batch methodology to the RBF soft sensor for the undisturbed case scenario.

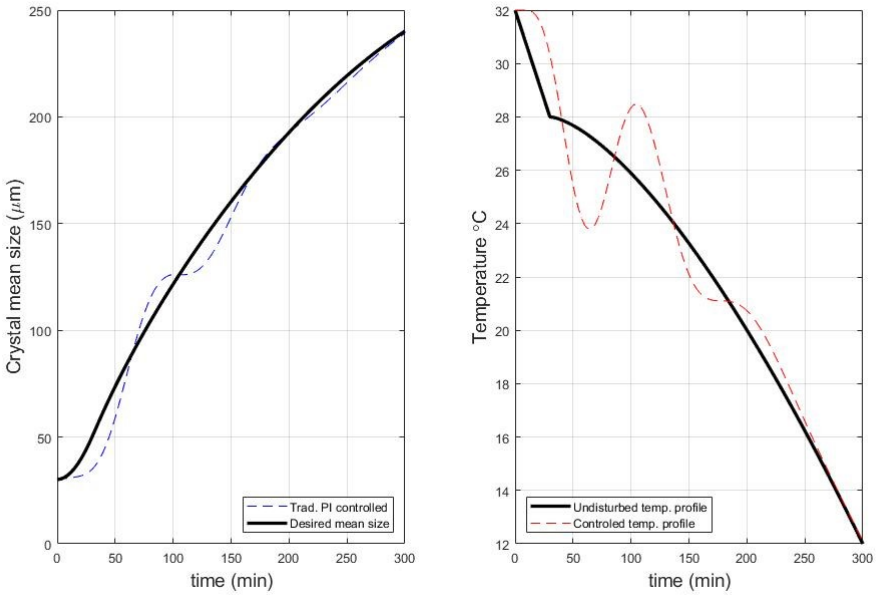

Figure S10. Crystal mean size (left) and temperature profile (right) obtained for the application of a traditional PI controller manipulating temperature from starting time, for the undisturbed case scenario.

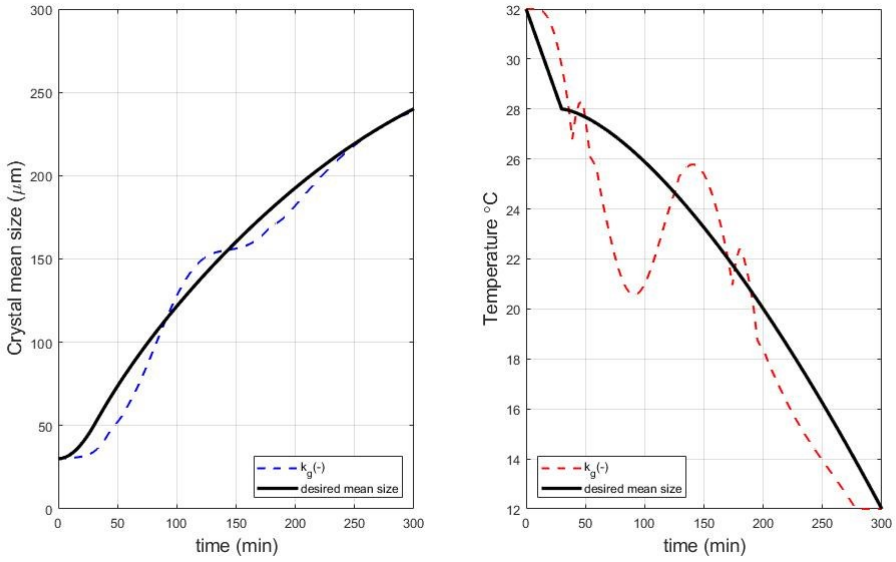

Figure S11. Crystal mean size dynamic profile (left) and temperature profile (right) with negative k_g disturbances, under RBF PI soft sensor control application with Golden Batch methodology.

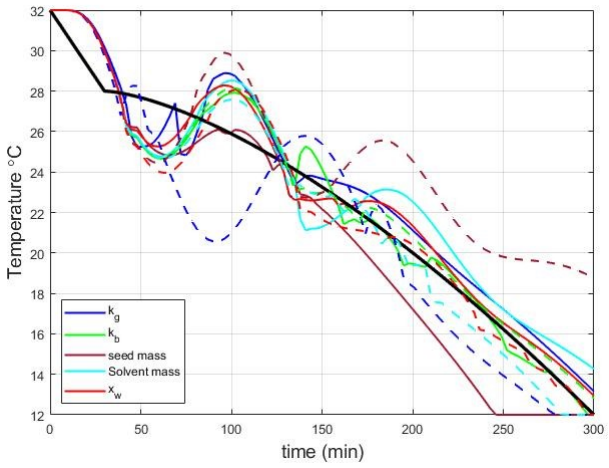

Figure S12. Controlled temperature profiles obtained for the application of the Golden Batch methodology to the RBF soft sensor with single step disturbances (positive disturbance: full line; negative disturbance: dashed line).

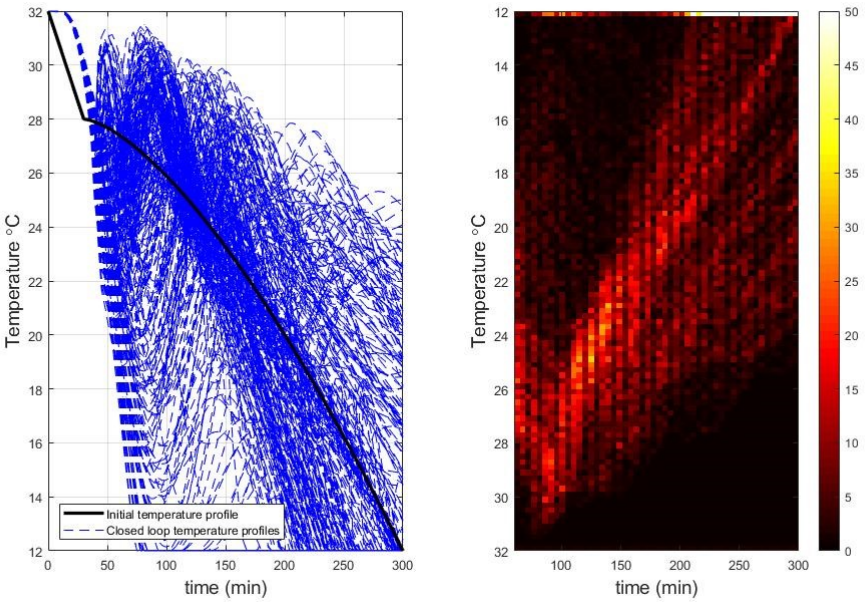

Figure S13. Controlled temperature profiles (left) and heat map of the temperature profiles over the course of the simulations (right) obtained for the application of the Golden Batch methodology to the RBF soft sensor with Monte Carlo sampling disturbances (300 LHS samples simulated).

Table S3. Final crystal mean size obtained for the PI soft sensor strategies.

		Crystal mean size μm				
		PI(30)	**MW**	**GW**	**PI**	**GB**
Undisturbed		238.7	***237.3***	239.1	239.1	239.6
k_g	+30%	238.9	***237.9***	***237.0***	239.2	239.3
	−30%	237.5	***235.2***	***234.6***	236.7	238.6
k_b	+32.5%	238.8	***236.9***	***236.0***	238.8	238.9
	−32.5%	238.8	***237.2***	***236.4***	239.4	239.5
m_{seed}	+25%	224.5	***224.1***	***224.1***	224.5	224.5
	−25%	239.6	***239.0***	***237.3***	241.1	240.3
$m_{solvent}$	+7.5%	239.5	***237.9***	***236.8***	239.8	***240.3***
	−7.5%	236.0	***235.2***	***234.6***	236.0	***235.9***
x_w	+45%	237.7	***237.3***	***236.5***	239.3	239.5
	−45%	237.3	237.6	***23.5***	239.6	238.0

0.2. S5.4 Cumulative distributions for the Monte Carlo simulations using the RBF PI soft sensor

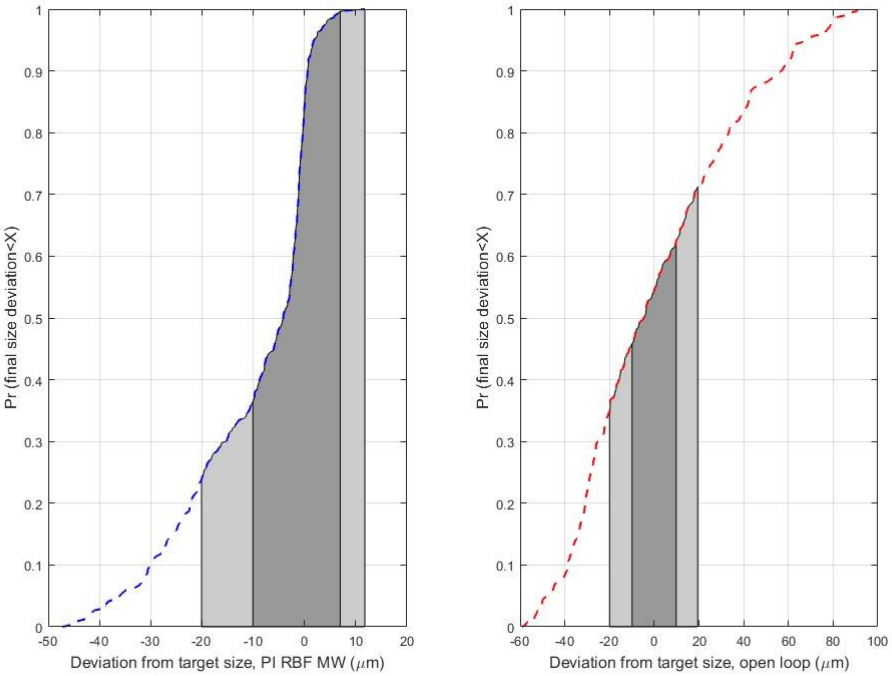

Figure S14. Cumulative distribution of the final mean size deviation for the RBF MW PI soft sensor (left) and open loop (right). The dark area represents a deviation within 10 μm, and the light area represents a deviation within 20 μm.

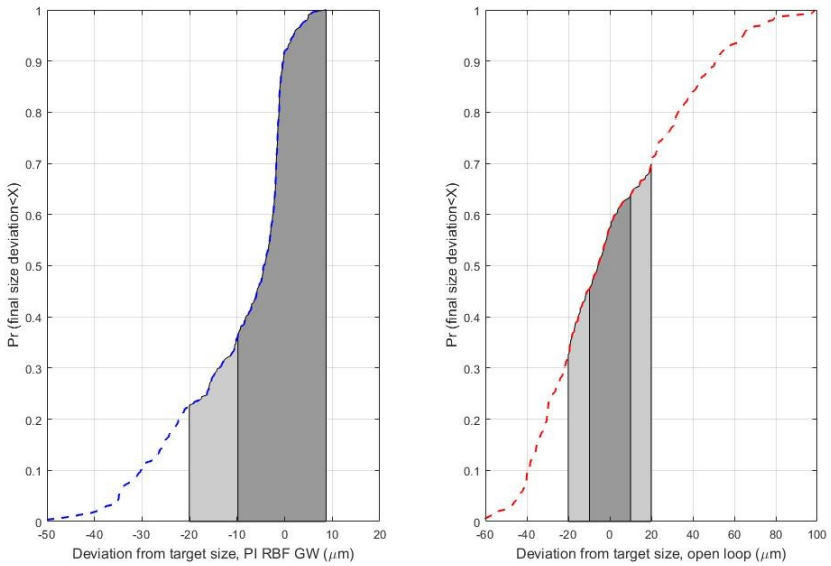

Figure S15. Cumulative distribution of the final mean size deviation for the RBF GW PI soft sensor (left) and open loop (right). The dark area represents a deviation within 10 μm, and the light area represents a deviation within 20 μm.

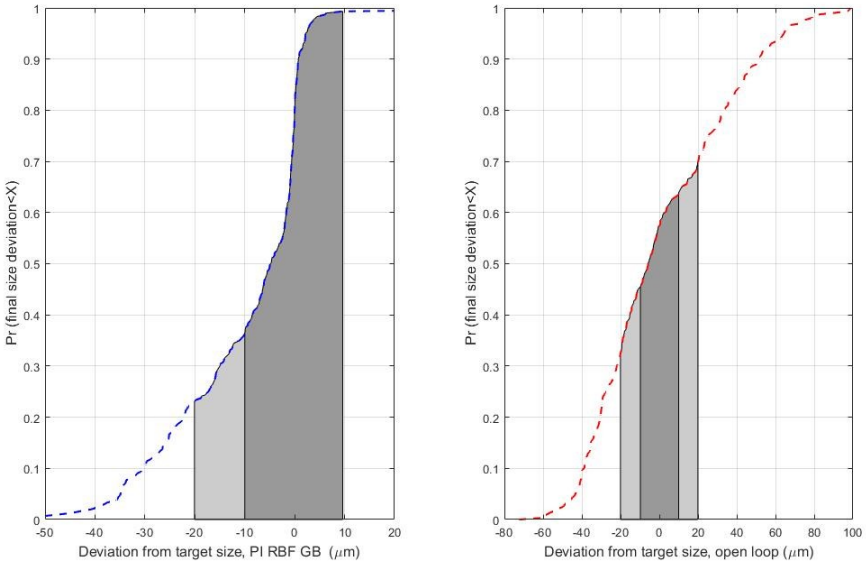

Figure S16. Cumulative distribution of the final mean size deviation for the RBF GB PI soft sensor (left) and open loop (right). The dark area represents a deviation within 10 μm, and the light area represents a deviation within 20 μm.

S6. Results obtained from RBF predictive control methodologies

S6.1. Undisturbed case scenarios for all the RBF methodologies

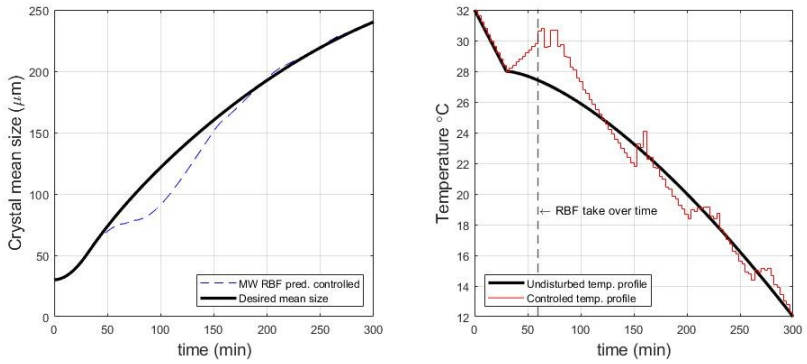

(a) Moving Window methodology.

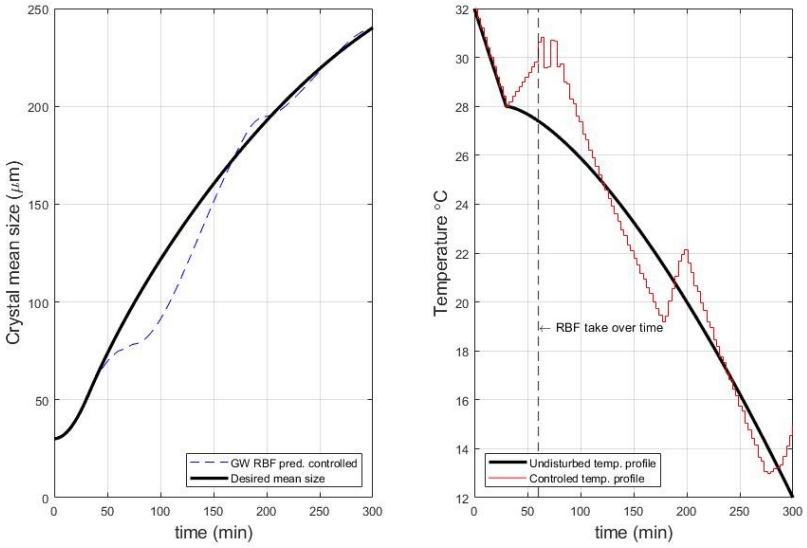

(b) Growing Window methodology.

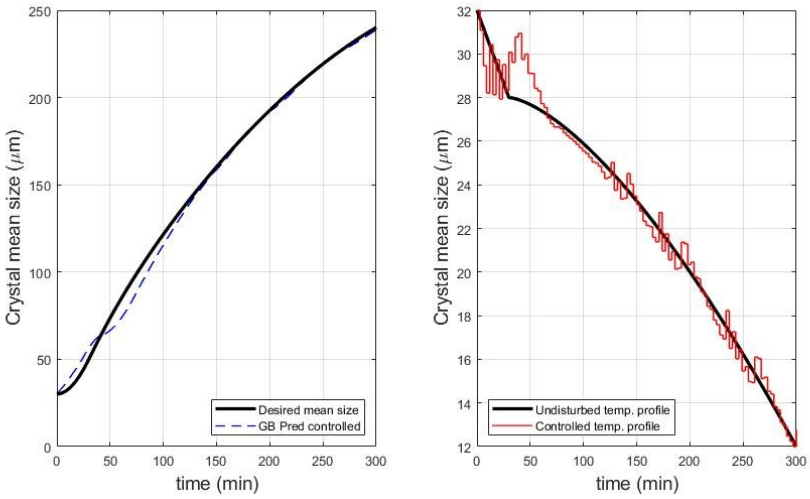

(c) Golden Batch methodology.

Figure S17. Crystal mean size (left) and temperature profile (right) obtained for the application of the RBF methodologies to the predictive control for the undisturbed case scenario.

S6.1. Mowing Window predictive control application

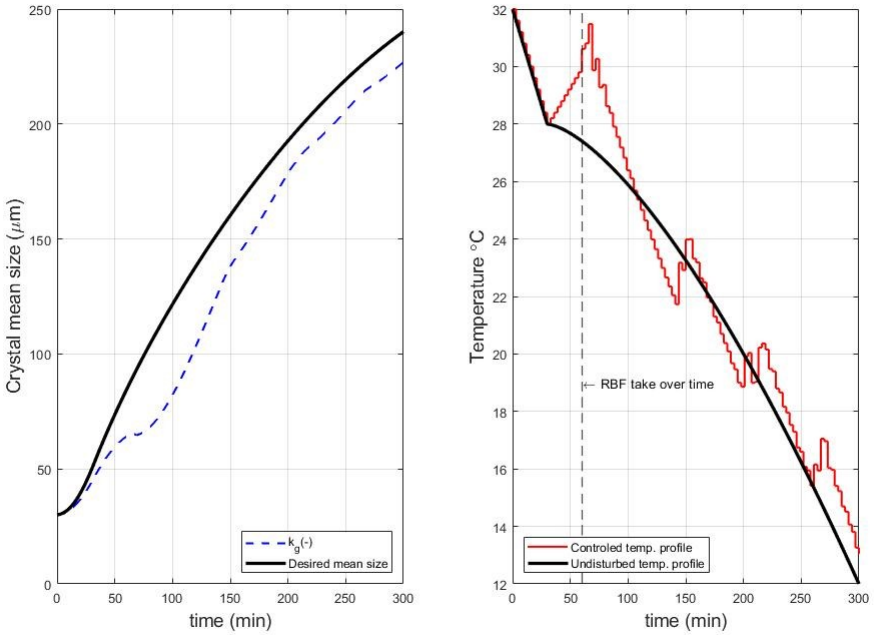

Figure S18. Crystal mean size dynamic profile (left) and temperature profile (right) with k_g negative disturbance, for the RBF Moving Window predictive control application.

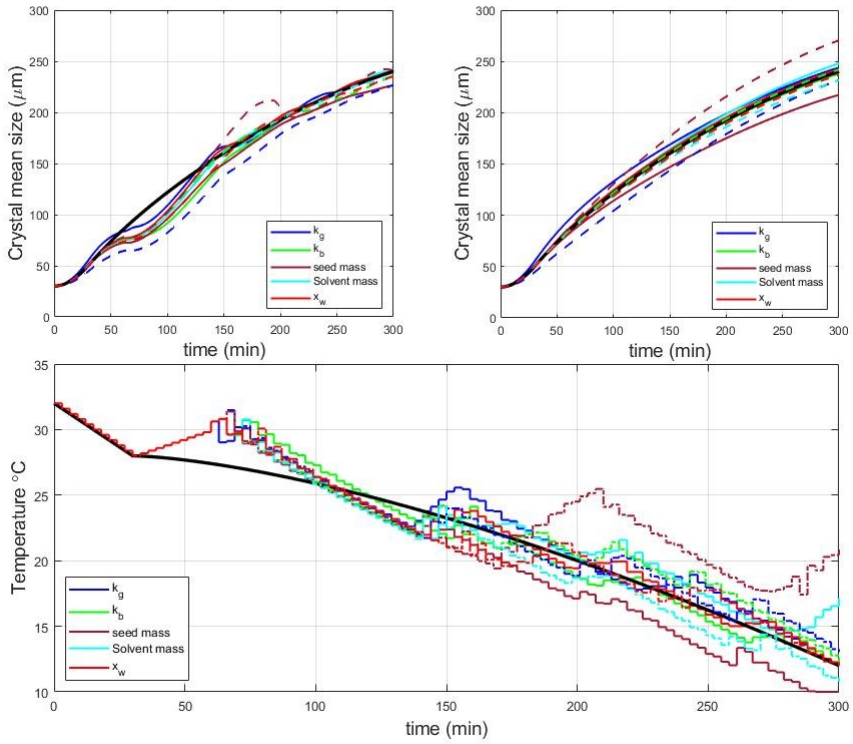

Figure S19. Controlled crystal mean size (top left) open loop crystal mean size (top right) and controlled temperature profiles (bottom) obtained for the application of the RBF predictive Moving Window control with single step disturbances (positive disturbance: full line; negative disturbance: dashed line).

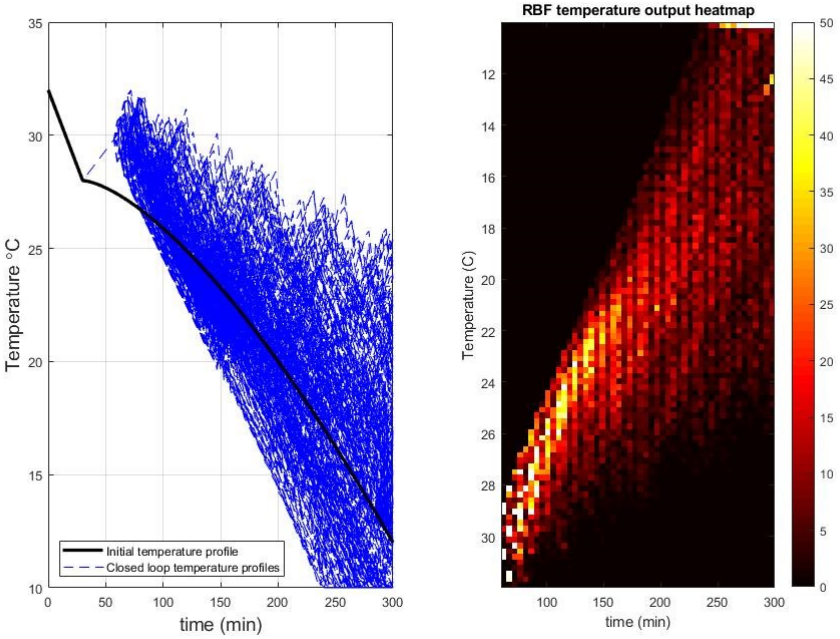

Figure S20. Controlled temperature profiles (left) and heat map of the temperature profiles over the course of the simulations (right) obtained for the application of the Moving Window methodology to the RBF predictive control with Monte Carlo sampling disturbances (300 LHS samples simulated).

S6.2. Growing Window predictive control application

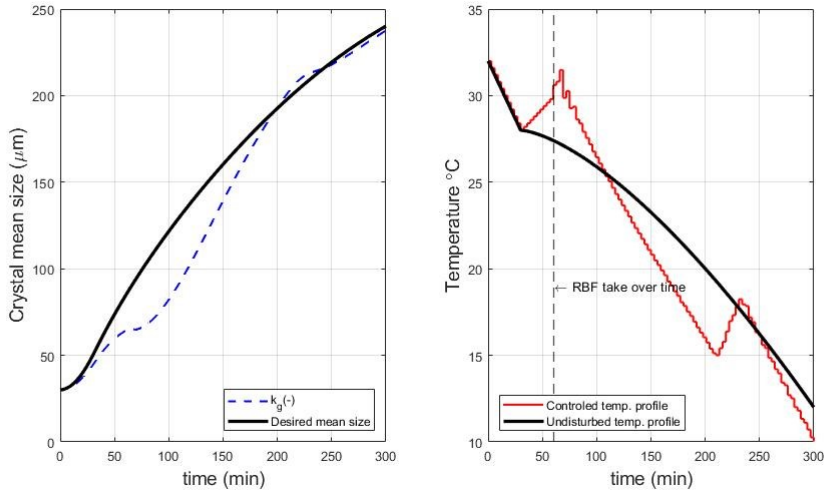

Figure S21. Crystal mean size dynamic profile (left) and temperature profile (right) with kg negative disturbance, under RBF Growing Window predictive control application.

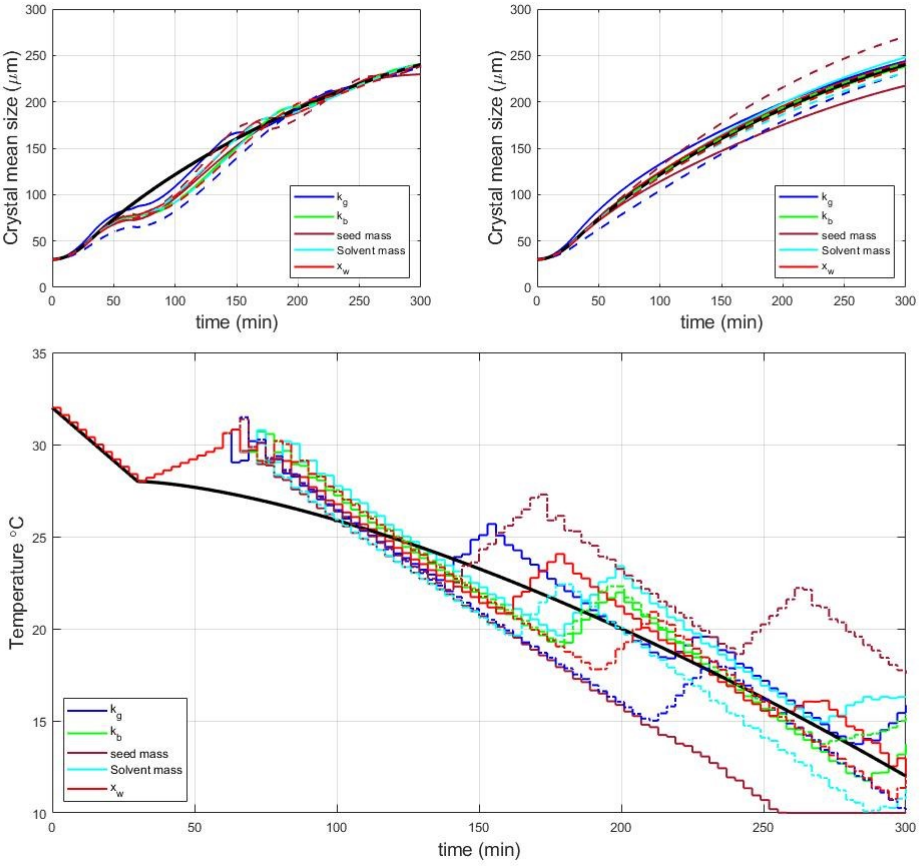

Figure S22. Controlled crystal mean size (top left) open loop crystal mean size (top right) and controlled temperature profiles (bottom) obtained for the application of the RBF predictive Growing Window control with single step disturbances (positive disturbance: full line; negative disturbance: dashed line).

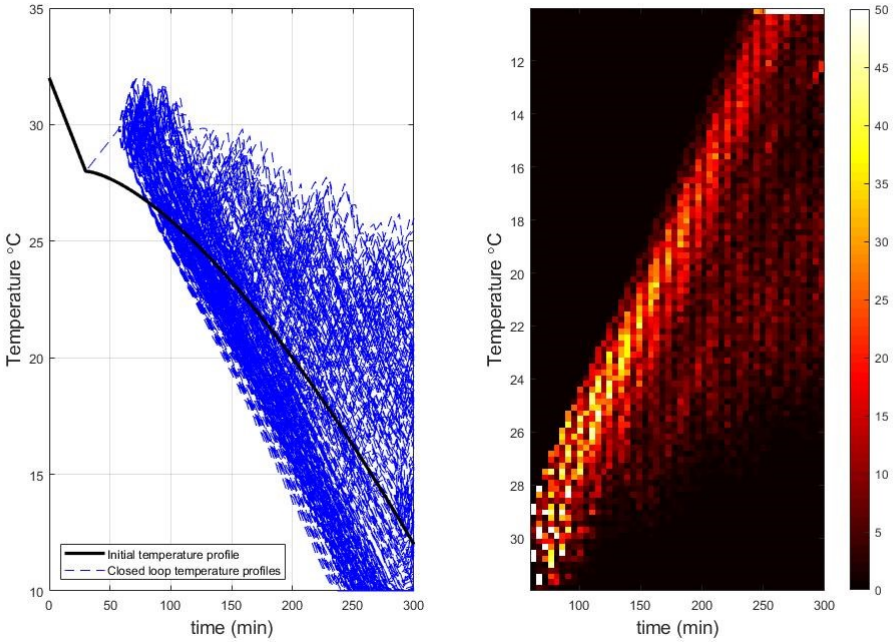

Figure S23. Controlled temperature profiles (left) and heat map of the temperature profiles over the course of the simulations (right) obtained for the application of the Growing Window methodology to the RBF predictive control with Monte Carlo sampling disturbances (300 LHS samples simulated).

S6.3. Golden Batch predictive control application

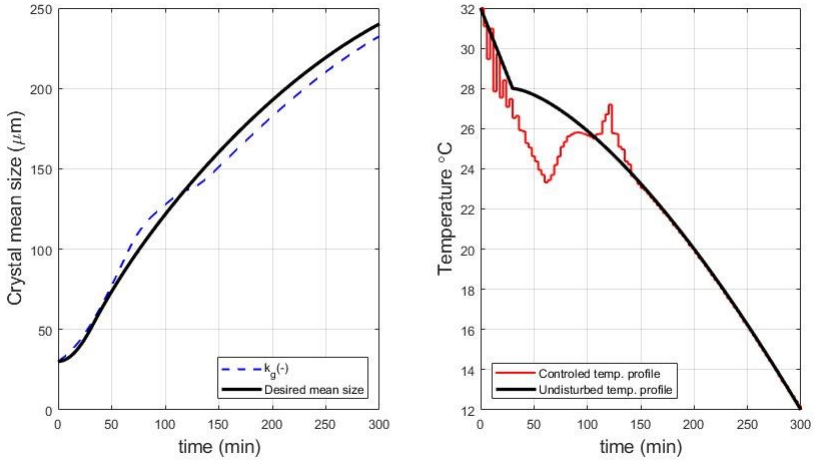

Figure S24. Crystal mean size dynamic profile (left) and temperature profile (right) with kg negative disturbance, under RBF Golden Batch predictive control application.

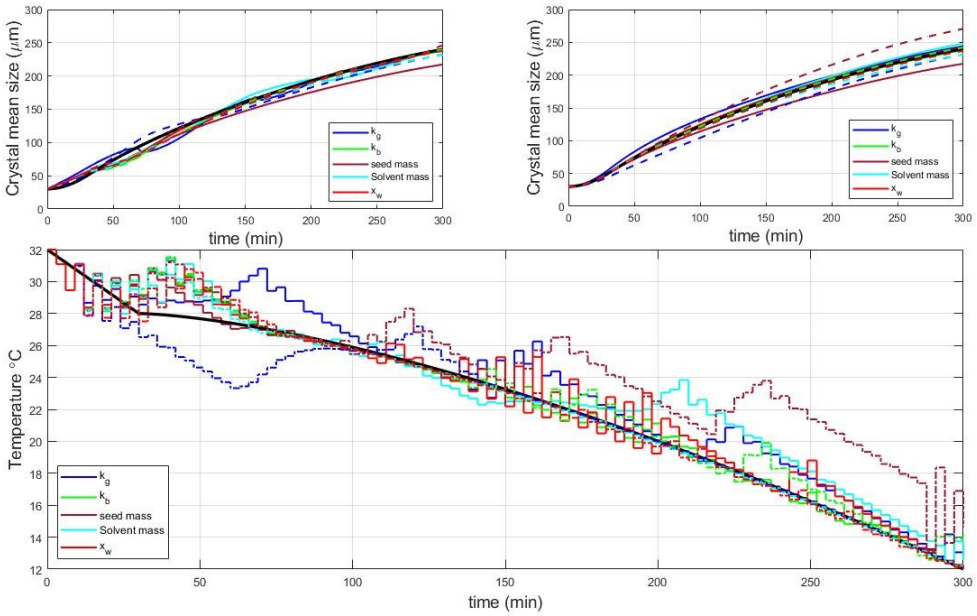

Figure S25. Controlled crystal mean size (top left) open loop crystal mean size (top right) and controlled temperature profiles (bottom) obtained for the application of the RBF predictive Golden Batch control with single step disturbances (positive disturbance: full line; negative disturbance: dashed line).

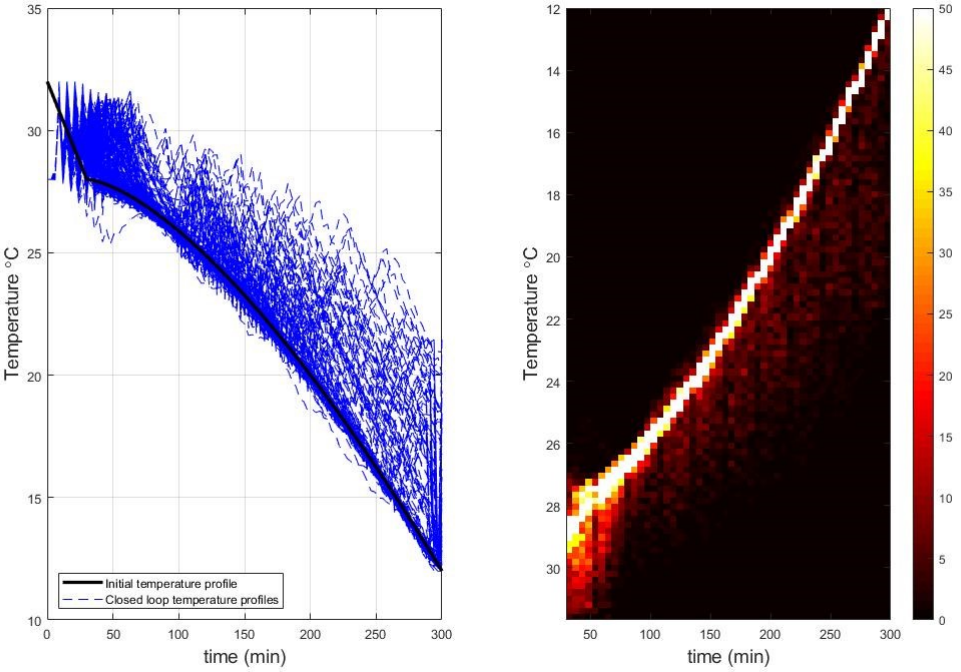

Figure S26. Controlled temperature profiles (left) and heat map of the temperature profiles over the course of the simulations (right) obtained for the application of the Golden Batch methodology to the RBF predictive control with Monte Carlo sampling disturbances (300 LHS samples simulated).

S6.4. Control performance evaluation of RBF predictive control methodologies

Table S4. Final crystal mean size obtained for the Predictive control methodologies.

		Crystal mean size [μm]		
	Disturbance	**MW**	**GW**	**GB**
Undisturbed		239.2	239.8	238.9
k_g	+30%	241.8	239.2	240.8
	−30%	226.9	237.6	232.5
k_b	+32.5%	238.8	240.7	238.1
	−32.5%	236.2	239.3	239.6
m_{seed}	+25%	226.5	229.6	217.4
	−25%	240.5	238.6	246.2
$m_{solvent}$	+7.5%	241.4	238.6	241.4
	−7.5%	240.3	239.9	232.0
x_w	+45%	235.4	240.1	240.7
	−45%	235.5	240.21	237.8

S6.5. Cumulative distributions for the Monte Carlo simulations using the RBF predictive control

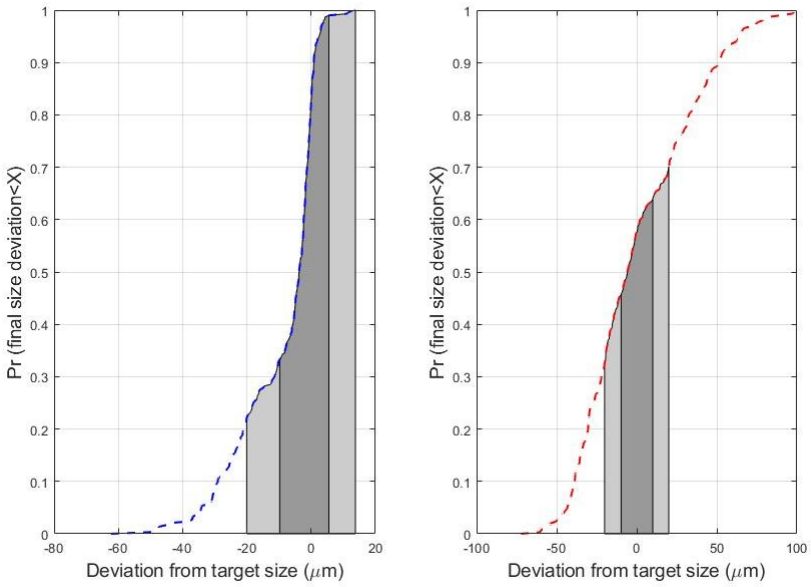

Figure S27. Cumulative distribution of the final mean size deviation for the RBF GW predictive control (left) and open loop (right). The dark area represents a deviation within 10 μm, and the light area represents a deviation within 20 μm.

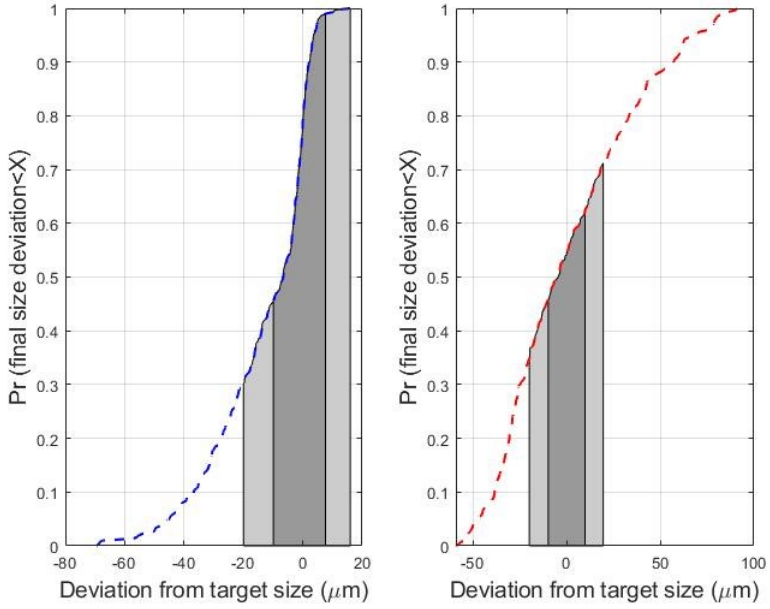

Figure S28. Cumulative distribution of the final mean size deviation for the RBF MW predictive control (left) and open loop (right). The dark area represents a deviation within 10 μm, and the light area represents a deviation within 20 μm.

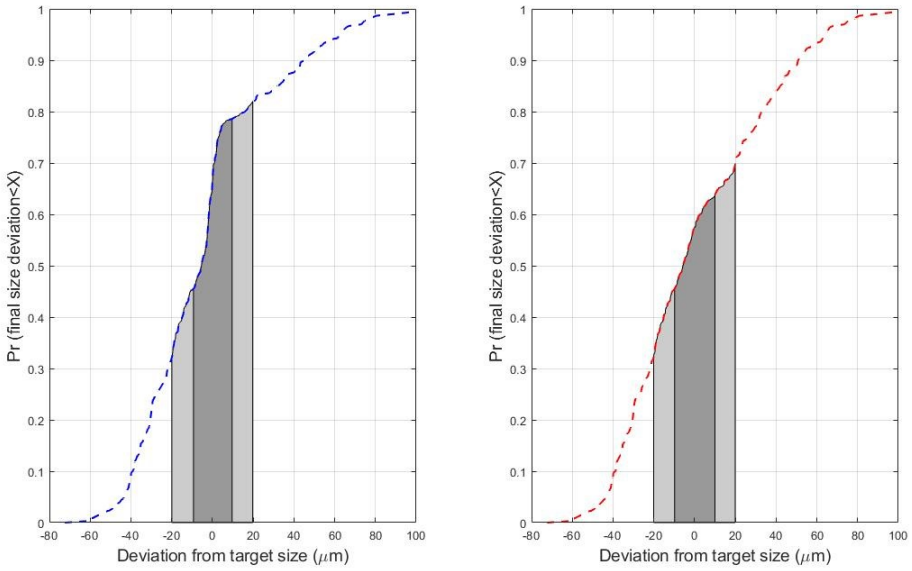

Figure S29. Cumulative distribution of the final mean size deviation for the RBF GB predictive control (left) and open loop (right). The dark area represents a deviation within 10 μm, and the light area represents a deviation within 20 μm.